Efficient HCN and H_2CO production in low-methane atmospheres driven by vertical mixing

Khalen Ferris,[1]★ N. J. Mayne,[1] M. Braam [2]
[1]Department of Physics and Astronomy, Faculty of Environment Science and Economy, University of Exeter, Exeter EX4 4QL, UK
[2]Center for Space and Habitability, University of Bern, Gesellschaftsstrasse 6, 3012, Bern, Switzerland

Accepted XXX. Received YYY; in original form ZZZ

ABSTRACT

Understanding the attainable yields of prebiotic molecules in planetary atmospheres is vital for studies of the origin of life on Earth, as well as for the detection and interpretation of biosignatures in exoplanet atmospheres. This work uses the 1-D photochemical kinetics tool, VULCAN, with the novel chemical reaction network, CRAHCN-O, to investigate the abundances of key biomolecule precursors in the atmospheres of the Archean Earth and TRAPPIST-1e. Across 45 Archean Earth configurations spanning K_{zz} from 0.01 - 100.0x present atmospheric levels and initial CH_4 abundances of 0.01-1.0%, vertically averaged HCN reaches 1 – 900 ppm, and H_2CO, 0.08 – 7.12 ppm. A reduced K_{zz} – CH_4 grid for TRAPPIST-1e shows yields of 0.8-19, and 0.4-5 ppm of HCN and H_2CO, respectively. Abundances of both species exhibit a non-monotonic relationship with K_{zz}. They initially increase for increasing K_{zz}, due to faster replenishment of CH_x radicals, before decreasing once excess mixing increases photolysis and weakens the photochemical shielding effect of C_2H_6 accumulation. The TRAPPIST-1e results show a higher optimum K_{zz}, likely due to increased CH_x photolysis under stronger Ly-α. High K_{zz} profiles are able to drive efficient HCN and H_2CO production even in CH_4-poor atmospheres with C/O ratios close to 0.5. This relaxes the typical requirements for a CH_4-rich atmosphere, and complicates the use of HCN and H_2CO as biosignatures. Future work should couple photochemistry to radiative transfer models and 3-D GCMs, as well as expanding the K_{zz} – CH_4 grid, to further understand the relationship between HCN/H_2CO production and K_{zz}/CH_4 and to account for horizontal mixing.

Key words: astrochemistry – planets and satellites: terrestrial planets – planets and satellites: atmospheres

1 INTRODUCTION

The origin of life on Earth remains an open question. Understanding how abiotic chemical processes can lead to the development of the first organisms is vital not only for our understanding of our own origins but also for assessing the potential for life to begin elsewhere in the universe. Additionally, our ability to characterise exoplanet atmospheres is limited, with previous research relying on hot Jupiters due to their size and relative proximity to their host stars (Veillet et al. 2023). Recent technological advances, such as the James Webb Space Telescope (JWST), allow for the observation of sub-Neptune and warm super-Earth atmospheres (Greene et al. 2016); however, we remain some distance from characterising the atmospheres of Earth-like exoplanets in Earth-like orbits. We therefore require advanced chemical models to advance our understanding of the atmospheric chemistry and prebiotic inventories of exoplanets, and hence plausible routes for life to emerge.

1.1 HCN and H_2CO as important biomolecule precursors

Chemical reactions, driven by temperature, UV radiation, lightning, or impacts, can provide significant abundances of molecules relevant to prebiotic chemistry (Cleaves 2012). Two compounds of particular interest are hydrogen cyanide (HCN) and formaldehyde (H_2CO). HCN is a key component in the synthesis of several important biomolecules, including nucleobases, amino acids and carboxylic acids (Ferris et al. 1996; Sanchez et al. 1967, 1968). Various formation pathways have been suggested for the formation of HCN: photochemical synthesis, detailed in §2.2 (Zahnle 1986; Tian et al. 2011; Rimmer & Rugheimer 2019); lightning-induced chemistry (Ardaseva et al. 2017); and interactions between C- and N-rich gases with subsurface water at hydrothermal vents (Rimmer & Shorttle 2019). Ruiz-Bermejo et al. (2013) summarises various experiments which identify purines and pyrimidines, important building blocks of RNA and DNA, in HCN polymers. The experiments vary greatly in terms of the time taken, ranging from a few hours to 27 years. Most of the experiments use HCN solutions as their starting point, with concentrations varying between 0.001 M and 14.6 M.

As originally described in Henry (1803), and recently discussed in Sander (2023), the solubility of a gas can be quantified by its Henry's law solubility constant, H_s, with units of M atm^{-1}. H_s is related to

★ E-mail: kf386@exeter.ac.uk

the aqueous concentration of the solute, C, and its partial pressure in the atmosphere, p by

$$H_s = \frac{C}{p} \quad (1)$$

where C and p have units of M and atm, respectively. For HCN at a reference temperature of 298.15 K, $H \approx 9.0$ M atm^{-1} (Burkholder et al. 2015, 2019). Therefore, to reach solutions with a concentration of 0.001 M, as on the lower end of the experiments discussed in Ruiz-Bermejo et al. (2013), 0.001M/(9.0M atm^{-1}) $\approx 1\times10^{-4}$ atm = 100 ppm of HCN would be required. Note that this is not necessarily the minimum abundance at which HCN is significant, with Rimmer & Rugheimer (2019) taking HCN production > 1 ppm as likely to be prebiotically important.

Weber (1998) demonstrates that a solution of 10 mM H_2CO and glycolaldehyde ($C_2H_4O_2$), reacting with ammonia (NH_3), yields alanine through "thioester" synthesis. Another important mechanism for prebiotic amino acid production is Strecker synthesis. Strecker synthesis involves heating a mixture of HCN, NH_3, and an aldehyde, such as H_2CO. This produces an amino nitrile, which yields an amino acid when hydrolysed. Millimolar concentrations of H_2CO are likely sufficient for Strecker synthesis. Following the same process as above, with $H_s = 3.2 \times 10^2$ M atm^{-1} (Burkholder et al. 2015, 2019), we find that H_2CO abundances are likely prebiotically significant above $\approx$ 3 ppm, corresponding to aqueous concentrations of a few mM.

1.2 The Archean Earth and TRAPPIST-1e

Life is believed to have originated on Earth during the Archean aeon (Lepot 2020), which spans 4.0-2.5 billion years ago (Ga). The aeon begins with the end of the Late Heavy Bombardment and continues until the Great Oxidation Event. As such, understanding the conditions of the Archean Earth atmosphere and climate, and the availability of important biomolecule precursors, is vital to origins of life research. Geological evidence can inform constraints on the Archean (Martini 1994; Johnson et al. 2014; Kadoya & Catling 2019), however continuous advancement of atmospheric and chemical models is required to push the field further (e.g. Zahnle 1986; Rimmer & Rugheimer 2019; Pearce et al. 2022), especially for the earliest Earth atmospheres.

The exact conditions of the atmosphere and its constituents are fundamentally driven by stellar radiation. Stellar models predict the luminosity of the Sun during the Archean to be 70-80% that of the present-day (Gough 1981), this is referred to as the faint young sun problem. Assuming no changes to the Earth's climate, this would result in a snowball Earth for much of the first 2 billion years of the planet's evolution. There is, however, sufficient evidence for the existence of liquid water and potentially life in the Archean (Feulner 2012). It is therefore thought that a reducing atmosphere with a greenhouse of: ammonia (NH_3), methane (CH_4), water vapour (H_2O), carbon dioxide (CO_2), and hydrogen sulphide (H_2S) is required (Feulner 2012).

The exact composition of this atmosphere is unknown. Catling & Zahnle (2020) discusses the Archean atmosphere in detail, and summarises constraints on atmospheric gases based on geological evidence and previous studies including photo- and lightning-induced chemistry, in Table 1. Estimates can also be made for the environmental temperature and pressure (de Wit & Furnes 2016; Som et al. 2016).

Aside from our own, the most studied planetary system is that of TRAPPIST-1 (Gillon et al. 2017; Grimm et al. 2018). The system is of particular interest to contemporary origins of life studies as it contains seven Earth-like planets, in size and mass. Three of the planets, TRAPPIST-1e, f, and g, are well within the habitable zone of their ultra-cool red dwarf host star, with low enough equilibrium temperatures for liquid water to exist on their surfaces (Gillon et al. 2017). TRAPPIST-1e has the highest Earth Similarity Index (ESI) of the habitable zone planets, at 0.85 compared to 0.68 and 0.58 for TRAPPIST-1f and g, respectively. The ESI describes how similar a planet is to Earth, with Earth having an ESI of 1.0, and a planet entirely different from Earth, 0 (Saha et al. 2018). TRAPPIST-1e's atmosphere is even more of an unknown than the Archean Earth's. Without geological evidence, or the ability to observe the atmosphere, it is difficult to place constraints on the composition, pressures and temperatures, and even existence of the atmosphere. Recent studies have considered several atmospheric scenarios including both land and aqua planets, often with N_2-dominated atmospheres, with varying levels of atmospheric CO_2 (Fauchez et al. 2020a; Krilanovic 2025).

1.3 Aims of this study

Studies of prebiotic chemistry likely require reducing atmospheric conditions. Previous studies on the photochemical production of HCN have emphasised the importance of CH_4-rich atmospheres with restrictions on the C/O ratio (e.g. Zahnle 1986; Rimmer & Rugheimer 2019), however, there are no prominent studies which focus on the impact of vertical mixing on HCN and H_2CO production. Additionally, whilst CRAHCN-O has been applied to the early Earth and Titan (Pearce et al. 2022, 2020b), it has not been used in VULCAN to study terrestrial atmospheres. In this work, we use the 1-D photochemical kinetics code VULCAN with the CRAHCN-O chemical reaction network (CRN) to simulate the chemistry of the Archean Earth and TRAPPIST-1e. We use these models to investigate the impact of CH_4 availability and vertical mixing in the atmosphere on HCN and H_2CO synthesis. We first describe vertical mixing and the photochemical production/destruction of HCN and H_2CO in Section 2. We then describe our methods and justify our planetary configurations in Section 3. We present our results in Section 4, where we show that there was likely sufficient production of atmospheric HCN and H_2CO for nucleobase/amino acid synthesis, potentially even in oxidising atmospheres. We also highlight vertical mixing as a mechanism to drive efficient HCN/H_2CO production in CH_4-poor, C/O $\approx$0.5 atmospheres; however, very high vertical mixing decreases the mixing timescale more than the reaction timescale, and hence harms HCN/H_2CO production. Finally, we draw conclusions and suggest paths for future work in Section 5.

2 THEORY

In this section we describe in more detail vertical mixing in planetary atmospheres. We also discuss the photochemical production of HCN and H_2CO.

2.1 Eddy diffusion coefficient

Vertical transport in 1-D is described by the eddy diffusion coefficient, K_{zz} and the molecular diffusion coefficient, D_i, both with units of cm^2 s^{-1}. The level at which $K_{zz} = D_i$ is referred to as the homopause. Within this regime, D_i is negligible and K_{zz} dominates. The characteristic mixing timescale is

$$\tau_K = \frac{H^2}{K_{zz}} \quad (2)$$

where H is the height of the homopause ($\sim$ 100 km for Earth). Atreya (1986) describes in full detail the derivation of this timescale from the continuity and flux diffusion equations. In §4 we refer to the Damköhler number (Da) as a qualitative tool to explain observed behaviours. This is the ratio of the characteristic timescale of a chemical reaction to τ_K (Bennett et al. 2019). We expect peak production rates to occur near Da = 1, where reactant replenishment from vertical mixing and chemical reaction rates balance.

2.2 Photochemical synthesis of HCN and H_2CO

When stellar radiation interacts with a planet's atmosphere, it either initiates chemical reactions or is converted into thermal energy. The process by which photons break apart molecules is referred to as photodissociation/photolysis, and is driven by the radiative flux, conventionally referred to as the actinic flux when passing through the atmosphere. The photolysis rate of a reaction can be determined from the integral of the actinic flux and the relevant absorption over the range of wavelengths of the radiation. This calculation is explained in full detail in §2.4 of Tsai et al. (2017).

HCN and H_2CO can both be produced photochemically in planetary atmospheres (Zahnle 1986; Pinto et al. 1980). The photolysis of N_2 produces atomic nitrogen, which is brought downward through vertical mixing. Here it reacts with CH_4 radicals to form HCN. In N_2-dominated atmospheres, with sufficient CH_4, the dominant production channels are $CH_3 + N \longrightarrow HCN + H_2$ and $^3CH_2 + N \longrightarrow HCN + H$ (Zahnle 1986). HCN is primarily destroyed via oxidation ($HCN + O \longrightarrow NCO + H$) and photolysis to CN + H.

Rimmer & Rugheimer (2019) demonstrates that efficient production of HCN is heavily reliant on the carbon-oxygen ratio (C/O): for C/O < 0.5, there is little HCN production even in CH_4 rich atmospheres; for 0.5 < C/O ≤ 1.5, there is significant HCN production, $1 - 10^3$ ppm, which increases with increased CH_4 availability; finally, for C/O > 1.5, HCN can reach > 0.1%, largely independent of atmospheric composition.

Photolysis of CO_2 and H_2O supplies atomic hydrogen and carbon monoxide (CO), which react to form HCO. This reacts with itself to form H_2CO. This sequence can be summarised as $CO_2 + 2\,H_2 \longrightarrow H_2CO + H_2O$, and is thought to be reliant on a reducing atmosphere (Pinto et al. 1980).

3 METHODS

In this section, we describe the photochemical model we are using: the photochemical kinetics code VULCAN with the CRAHCN-O CRN. We then describe and justify choices made for our planetary configurations.

3.1 Photochemical Model

We use VULCAN to simulate prebiotic chemistry in the Archean Earth and TRAPPIST-1e atmospheres. VULCAN is an open-source 1D photochemical kinetics code which calculates the number density of chemical species over time by solving a set of mass continuity equations (Tsai et al. 2017, 2021). The CRN used defines the interactions between different species. VULCAN was initially developed for studying gaseous chemistry from 500 to 2500 K with a reduced C-H-O CRN (Tsai et al. 2017). It was updated in Tsai et al. (2021) to include C-H-N-O-S CRNs and photochemistry. Reactions are driven by the incident stellar radiation, background pressure-temperature and vertical mixing profiles, and upper/lower boundary conditions for constituent fluxes. VULCAN has been used previously for hot Jupiters (Coulombe et al. 2023; Tsai et al. 2023); however, there are few prominent studies with a focus on Earth-like planets. VULCAN uses data on photoabsorption, photodissociation, and photoionisation cross sections from the Leiden Observatory database (Heays et al. 2017). The full list of photolysis reactions included in VULCAN is shown in Table 6 of Tsai et al. (2021).

We use the novel reaction network CRAHCN-O (Pearce et al. 2020a). CRAHCN-O is an oxygen extension to CRAHCN, a consistent reduced atmospheric hybrid chemical network, and can be used to simulate HCN and H_2CO production in CO_2-, N_2-, H_2O-, CH_4-, and H_2-dominated atmospheres. The network contains rate coefficients for 126 total reactions, 39% of which are validated against experimental data. For the cases without valid experimental results, quantum calculations were used to determine rate coefficients. When compared to the experimental rate coefficients, the calculated coefficients are often within a factor of 2, and the vast majority are within an order of magnitude (Pearce et al. 2020a). Braam et al. (in prep.) discusses the implementation of CRAHCN-O into VULCAN and compares it to the default NCHO network. It is shown that for C/O ratios > 0.5, in the presence of CH_4, the abundance profiles diverge in the photochemical regions. This is caused by hydrocarbon photochemical shielding, as CRACHN-O accumulates ethane (C_2H_6), which is photochemically active, whereas NCHO accumulates butatrienyl (C_4H_3) and propyne (C_3H_4), which are not.

3.2 Planetary Configurations

3.2.1 The Archean Earth

We initially use a 1 bar atmosphere comprised of 89% N_2, 10% CO_2, and 1% CH_4 for the Archean Earth. This is in line with previous studies (Zahnle 1986; Rimmer & Rugheimer 2019; Eager-Nash et al. 2024). Both CRAHCN-O and SNCHO are used for the initial Archean Earth simulations to benchmark our VULCAN CRAHCN-O model. Previous work (Zahnle 1986; Rimmer & Rugheimer 2019) has highlighted the CH_4 dependence of HCN production in N_2-dominated atmospheres. We hence run further simulations of the Archean keeping CO_2 fixed at 10% and varying CH_4 from 100 ppm to 1%, with N_2 making up the rest in each case, to test this dependence in our model. As well as the atmospheric composition, the stellar flux profile of a planet's host star and atmospheric escape have a significant impact on the photochemistry which occurs in the upper atmosphere.

Claire et al. (2012) combines data from the Sun and solar analogues, and standard solar models, to estimate the UV and X-ray, and visible and infrared fluxes, respectively. These estimates are valid from 0.1 nm to 160 μm, and from 0.6 - 6.7 Ga. The numerical parametrisation used is validated by Monte Carlo analysis of uncertainties in stellar age and flux, as well as through comparison to the solar proxies κ^1Cet and EK Dra. For our simulations of the Archean Earth, we utilise a stellar flux profile, computed in Claire et al. (2012), for the 3.8 Ga Sun, which is compared to the present-day stellar flux in Fig. 1a. VULCAN requires the stellar flux profiles to describe the flux at the stellar surface, and so the inverse-square law is used to scale the profile appropriately.

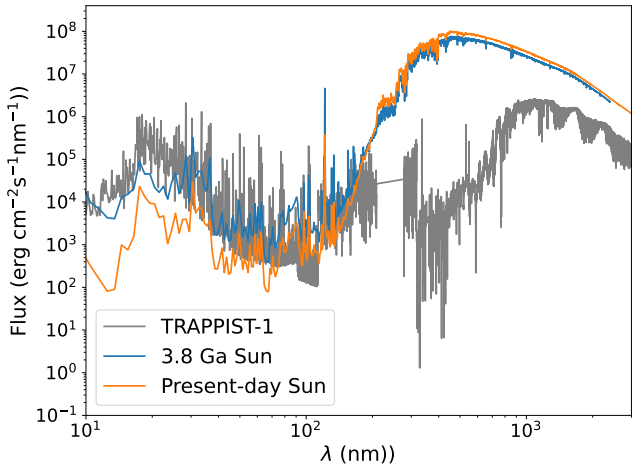

(a)

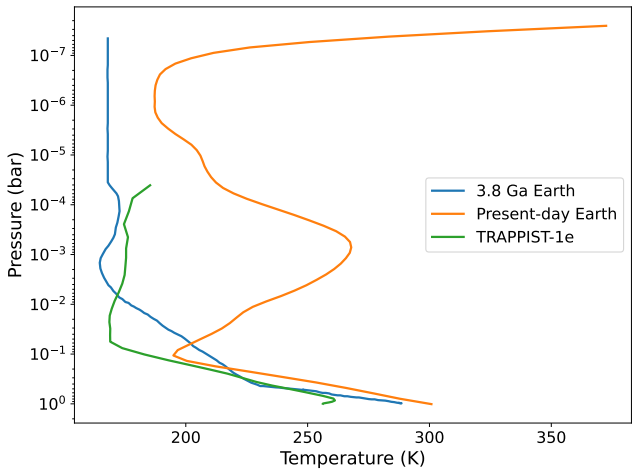

(b)

Figure 1. Panel (a) shows the stellar flux distribution, at the stellar surface, of TRAPPIST-1, and the 3.8 Ga and present-day Sun and (b) shows the comparison between the P-T profiles of the present-day and Archean Earth, and TRAPPIST-1e.

Eager-Nash et al. (2024) generates vertical profiles for both pressure and temperature for the 3.8 Ga Earth atmosphere (see Fig. 2 of Eager-Nash et al. (2024)). We extract these profiles using PlotDigitizer (available at: `https://plotdigitizer.com/`, last accessed: 18 August 2025) and combine them to create a temperature-pressure profile for the Archean (shown in Fig. 1b). We run initial simulations with the present-day K_{zz} profile (Fig. 2), which is provided in VULCAN, and taken from Massie & Hunten (1981). The K_{zz} profile of the Archean atmosphere is a source of uncertainty. To this end, we run simulations with K_{ZZ} scaled to: 0.01x, 0.10x, 0.25x, 0.50x, 0.75x, 1.0x, 5.0x, 10.0x, and 100.0x present atmospheric levels (PAL), to investigate the impact of vertical mixing on the production of prebiotically relevant compounds.

We use the present-day Earth's lower boundary condition of species flux with sulphur species removed to accommodate CRAHCN-O. These fluxes are outlined in Table 1, following Tsai et al. (2021). At the upper boundary we apply diffusion-limited escape for H and H_2, and zero-flux for all other species. The atmosphere is split into 120 vertical layers, with pressure ranging from $1-5\times10^{-7}$ bar.

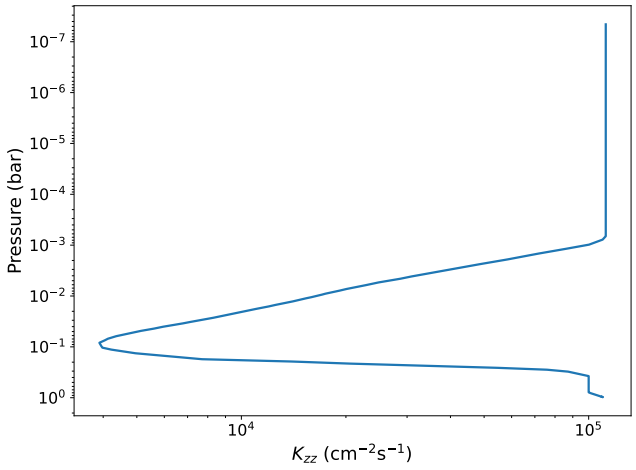

Figure 2. K_{zz} profile of the present-day Earth, as in Massie & Hunten (1981) and default in VULCAN.

Table 1. The default lower boundary condition for the present-day Earth in VULCAN, with sulphur-containing species removed. v_{dep} refers to the surface deposition velocity; the rate at which particles are deposited to the planetary surface (Ysebaert et al. 2021).

Species	Flux (cm^{-2}s^{-1})	v_{dep} (cm s^{-1})
CO_2	3.7×10^{11}	0.03
CH_4	1.6×10^{11}	0.00
NO	1.3×10^{10}	0.001
NH_3	1.5×10^{9}	1.00
N_2O	2.3×10^{9}	10^{-4}
NO_2	0	0.01
NO_3	0	0.10
HCN	1.7×10^{8}	0.13
CH_3CN	1.3×10^{8}	0.13
HNO_3	0	4.00

3.2.2 TRAPPIST-1e

Our TRAPPIST-1e simulations also use the present-day Earth K_{zz} profile. We adjust stellar and planetary radii, the surface gravity, and the diurnal average of solar flux to account for the fact that TRAPPIST-1e is tidally locked. We use the most recent observational data from the MUSCLES survey from the MAST Portal (France et al. 2016) for our stellar flux profile. This is also shown in Fig. 1a for comparison to the 3.8 Ga and present-day Sun.

Atmodeller (Bower et al. 2025) is used to inform our decisions on the atmospheric composition of TRAPPIST-1e. Atmodeller is an open-source Python package to predict atmospheric compositions of terrestrial- and sub-Neptune planets, which leverages JAX (Bradbury et al. 2018) for high-performance computation. Mass exchange between planetary interiors and their atmospheres occurs during a planet's magma ocean stage. The planet's volatile budget, chemical equilibria, and gas/fluid solubility in molten rock determine the mass and initial chemical composition of the atmosphere. Gas-phase reactions, condensation, and thermodynamic balance between species then modify the atmosphere as it cools. Atmodeller begins with a molten TRAPPIST-1e just after formation, at a temperature of 1800 K, and a Monte Carlo simulation is used to predict the atmospheric composition in equilibrium with the magma ocean. The volatiles dissolved in the interior are then removed, and new abundance constraints are calculated. The atmosphere is then collapsed to

280 K, which is roughly the equilibrium temperature of TRAPPIST-1e. Bower et al. (2025) finds that in the magma ocean stage, the atmosphere of a TRAPPIST-1e-like planet is often dominated by CO, evolving to CO_2-rich after isochemical cooling to 280 K. The atmospheric surface pressure is predicted to be ~ a few hundred bar. Around 40% of simulations predict that liquid water, graphite, α-sulphur, and ammonium chloride are all extant, which is important for surface habitability (Bower et al. 2025).

The TRAPPIST-1 Habitable Atmosphere Intercomparison (THAI) (Fauchez et al. 2020b; Sergeev et al. 2022; Fauchez et al. 2022) aims to quantify the climate impact of differences in general circulation models for TRAPPIST-1e. In this work, we utilise a temperature-pressure profile from the THAI data. We use the Hab1_LMDG dataset, which is for an ocean-only atmosphere with 1 bar of N_2 and 400 ppm of CO_2. As we are using this temperature-pressure profile, we are unable to use the most common Atmodeller result for our atmospheric composition, as the pressure and CO_2 levels are too high. However, one of the Atmodeller simulations predicts an atmosphere of 0.7 bar N_2, ~300 ppm CO_2, and ~2200 ppm CH_4. We use these mixing ratios for a 1-bar atmosphere for our simulations of a TRAPPIST-1e-like planet. Finally, we use a present-day Earth K_{zz} profile, as well as the same boundary conditions and atmospheric escape settings. As with the Archean Earth, we investigate the CH_4 availability dependence of HCN production in the TRAPPIST-1e atmosphere.

4 RESULTS AND DISCUSSION

In this section, we first compare abundance profiles for the Archean Earth produced using CRAHCN-O and the VULCAN network SNCHO. We then use CRAHCN-O to study and discuss the formation of HCN and H_2CO for 45 different atmosphere configurations. We vary the amount of CH_4 available for thermo- and photo-chemical reactions, as well as the K_{zz} profile of the atmosphere. We then briefly discuss the production of HCN and H_2CO in an oxidising, CO_2-dominated atmosphere with a K_{zz} at 10.0x PAL, for a planet in an Earth-like orbit around the 3.8 Ga Sun. Finally, we consider the atmospheric chemistry of TRAPPIST-1e for a reduced grid of experiments before discussing the limitations of this study.

4.1 CRAHCN-O vs SNCHO

In the initial CRAHCN-O simulation we see a significant increase in C_2H_6 abundance to >9,000 ppm from just 26.3 ppm for the SNCHO simulation. As discussed in Braam et al (in prep.), C_2H_6 accumulates in CRAHCN-O and is photochemically active, whereas in SNCHO we see a build up of C_3H_4 and C_4H_3, which are not. As a result the C_2H_6 in the CRAHCN-O simulation is able to effectively shield other species from photolysis. We therefore also see an increase in CH_4, CO_2, and H_2O abundances. The higher CH_4 abundance drives an increase in HCN production, which is also shielded from photolysis by C_2H_6. This comparison between the networks is shown in Fig. 3.

4.2 Prebiotic synthesis in the Archean Earth atmosphere

4.2.1 HCN production

We demonstrate the impact of varying CH_4 availability and K_{zz} by plotting the HCN abundance profile in each case (Fig. 4). For low vertical mixing, K_{zz} = 0.50x, 0.75x PAL, the impact of low CH_4 availability is clear. For initial CH_4 mixing ratios of 0.01, 0.05, and 0.10%, there is very little HCN production with abundances ranging between $\sim 10^{-3}$ and 0.20 ppm. However, when we increase the initial CH_4 availability to 0.5% we see a significant increase in HCN production, with abundances now reaching just under 400 ppm. This is in line with previous studies (Zahnle 1986; Rimmer & Rugheimer 2019), which suggest efficient HCN production requires significant CH_4 availability to achieve a high enough C/O ratio, normally from the ratio of CO_2 and CH_4 abundances.

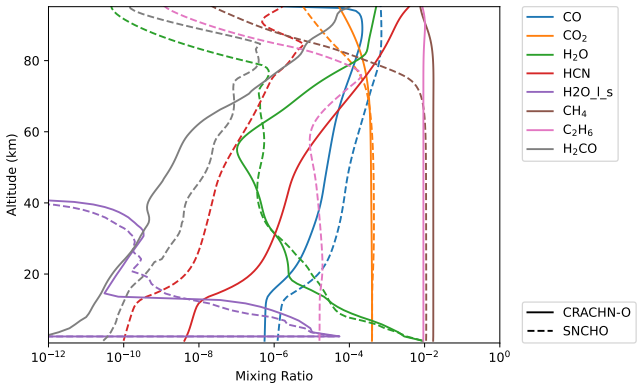

Figure 3. Abundance profiles of the Archean Earth with an initial composition of 89% N_2, 10% CO_2, and 1% CH_4, with the CRAHCN-O (solid line) and SNCHO (dashed line) chemical networks.

The K_{zz} = 1.0x PAL case, shown in Fig. 4(c), exhibits two unexpected behaviours. Firstly, the HCN abundance profile in the 0.05% CH_4 case decreases suddenly to mixing ratios considerably below the 0.01 and 0.10% cases between ~10 – 50 km. This may be caused by the averaging of mixing ratios in log scale. When taking vertical averages of the HCN abundance in each case, we see the expected behaviour: there is more HCN accumulation in the 0.10% CH_4 case than in the 0.05% CH_4 case, which has more HCN than the 0.01% CH_4 case.

We also see much higher HCN production in the 0.50% CH_4 simulation than in the 1.0% CH_4 simulation, with the former having a vertical average of 911 ppm whilst the latter, only 337 ppm. Interestingly, the simulation with an initial abundance of 0.50% CH_4 finishes with a CH_4 mixing ratio of 2.1%, whereas the 1.0% initial CH_4 simulation finishes with a CH_4 mixing ratio of only 1.6%. The increased availability of CH_4, and hence the CH_x species required for HCN synthesis, is likely what leads to more efficient HCN production in the lower initial CH_4 simulation; however, it is unclear what causes the difference in CH_4 availability.

The K_{zz} = 1.0x PAL case seems to show the transition from HCN production being primarily in the photochemical regions of the atmosphere, as shown for low K_{zz}, to being more evenly distributed throughout the atmosphere, as shown for high K_{zz}. The use of a finer grid of K_{zz} values, particularly between 1.0x and 5.0x PAL, would improve our understanding of this transition.

As we increase the K_{zz} profile (see Fig. 4 (d - f)), we see a decrease in the CH_4 dependency of HCN production. This leads to abundances of HCN well over the significant 1 ppm mark stated in Rimmer & Rugheimer (2019), even for an initial CH_4 abundance of 100 ppm. The HCN abundances produced in each simulation are shown in a grid, as a function of K_{zz} and the initial CH_4 abundance, in Fig. 5. There are three key points illustrated in the grid: A) we see significant HCN production (>1 ppm) in low-CH_4 atmospheres, provided there is sufficiently high vertical mixing, B) for each initial CH_4 abundance there is a vertical mixing profile above which we see a decline in

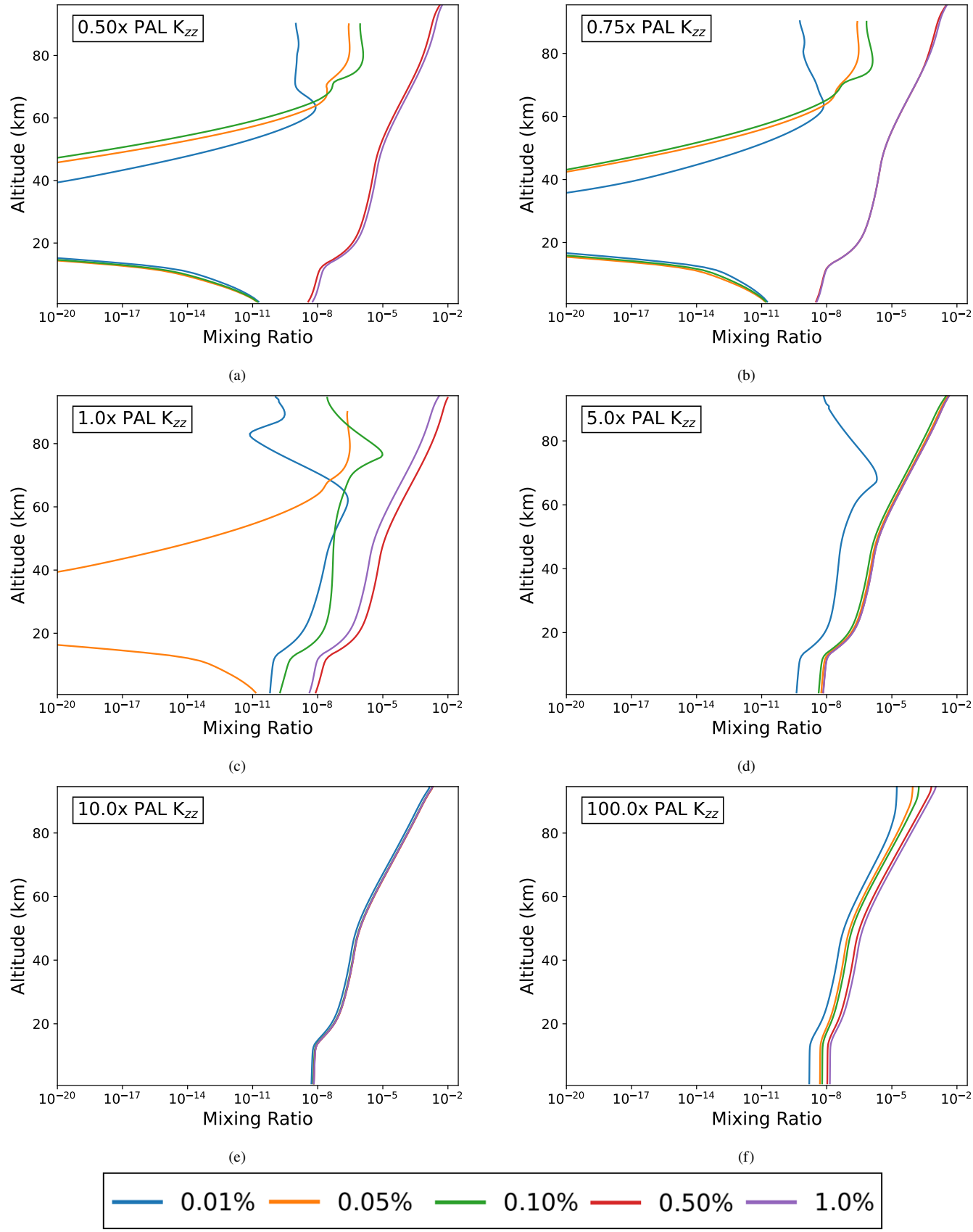

Figure 4. HCN abundance profiles for varying initial CH_4 abundance and K_{zz} profiles.

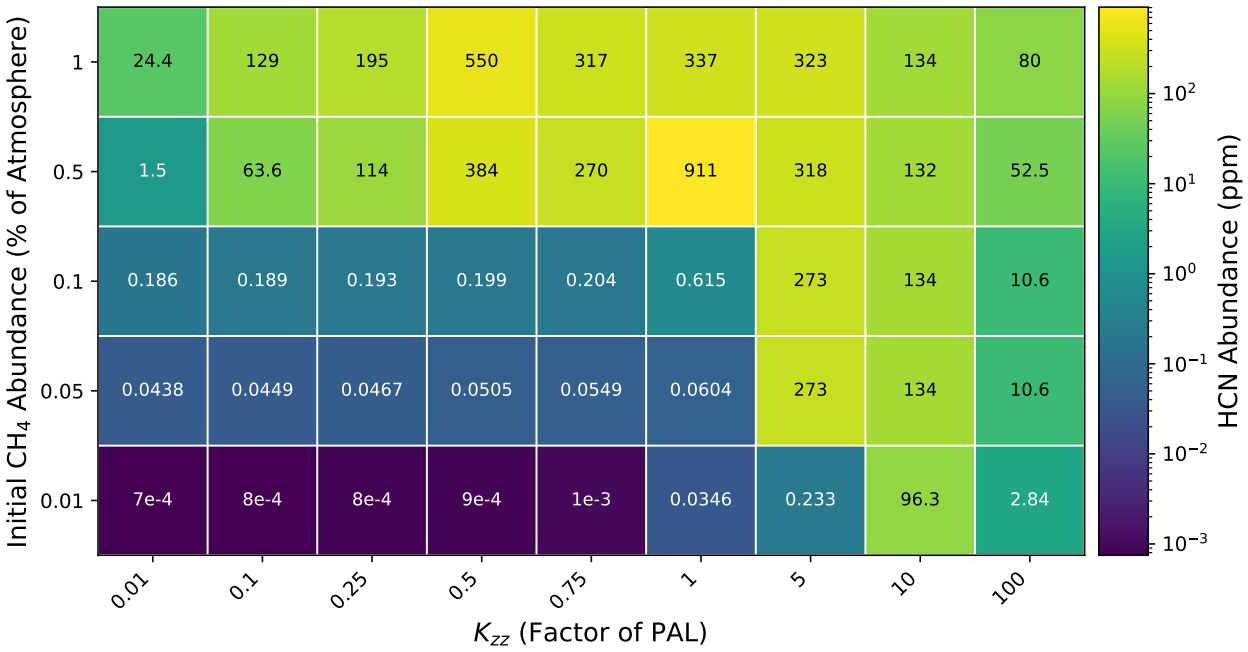

Figure 5. Vertically averaged HCN abundance for the full grid of Archean Earth simulations. Each square on the grid represents a simulation with a specific K_{zz} and initial CH_4 abundance value. The heat-map represents HCN abundance, with the values for each simulation shown in the squares in ppm.

HCN production, and C) 26 out of 45 configurations produce HCN abundances above the significant 1 ppm level stated in Rimmer & Rugheimer (2019), including a number of simulations with low CH_4 abundances and C/O ratios very close to 0.5. Additionally, 17 of 45 have HCN yields >100 ppm, and thus above the threshold required for rain-out of >1 mM aqueous HCN via Henry's law (see §1.1)

To understand how vertical mixing is able to drive efficient HCN production in low-CH_4 atmospheres we consider the most abundant species and their mean altitudes (Fig. A1), as well as the reaction rates of the most important production/destruction pathways for several species (Fig. A2). We first compare simulations with an initial CH_4 abundance of 0.01%, and K_{ZZ} profiles of 1.0x and 10.0x PAL. These simulations produced 0.0346 and 96.3 ppm of HCN, respectively.

In the high K_{zz} case there is more replenishment of CH_x species to the upper, photochemical region of the atmosphere. This acts to increase HCN production, but also significantly increases the rates of several key reactions for forming C_2H_6 such as $C_2H_4 + H_2 + H \longrightarrow C_2H_6 + H$, $CH_4 + C_2H_4 + H \longrightarrow C_2H_6 + CH_3$, and $CH_3 + CH_3 + M \longrightarrow C_2H_6 + M$. In the final reaction, M is some arbitrary molecule that acts to take away excess kinetic energy. This increased C_2H_6 abundance acts to further increase HCN abundances by shielding CH_4 and HCN from photolysis, allowing them to accumulate. Additionally, the increased K_{zz} profile leads to a decrease in the availability of atomic and molecular oxygen (O/O_2) in the atmosphere, hence decreasing the rate of HCN oxidation.

This decrease in O/O_2 is due to a few key mechanisms. Firstly, there is an increased abundance of hydrocarbons such as CH_3, C_2H_6, and H_2CN, which are all good oxygen sinks. O/O_2 that forms in the upper atmosphere is also brought closer to the surface due to the increased mixing and so survives for less time than if it were allowed to remain in the upper regions of the atmosphere. Finally, the increased CH_4 and C_2H_6 shields oxygen-containing species such as CO_2, H_2O, and NO_x from photolysis reactions, which would produce O. This comparison was also carried out for initial CH_4 abundances of 0.05, 0.10, 0.50, and 1.0%, which corroborated these results.

As the K_{zz} profile increases further, the abundance of important precursors including CH_4 and C_2H_6 decreases, and their mean altitudes increase. Comparison of reaction rate plots for the K_{zz} = 10.0 and 100.0x PAL cases shows that there is a decrease in reaction rates for several key production pathways of both CH_4 and C_2H_6. Furthermore, there is a significant increase in reaction rates for the destruction of these species. Due to the lower abundance and increased mean altitude of C_2H_6, it becomes less effective at shielding other species. As altitude increases, the atmosphere thins, and so a high ppm at high altitudes of e.g. C_2H_6 corresponds to fewer molecules of C_2H_6 than a high ppm at lower altitudes. The lower abundance and increased mean altitude of C_2H_6 act to decrease the effectiveness of its photochemical shielding. This leads to an increase in CH_4 and HCN photolysis.

As shown in Fig. 5, as we increase the initial CH_4 abundance of the atmosphere, the optimum K_{zz} profile for HCN production shifts lower. As discussed in §2.1, HCN production will be most efficient when Da = 1, i.e. the vertical mixing timescale and the chemical reaction rate are equal. As the K_{zz} profile increases, the mixing timescale decreases. As we have demonstrated, it also increases the availability of CH_x species in the atmosphere, and hence decreases the reaction rates of important reactions in the synthesis of HCN. We therefore see Da = 1, and hence peak HCN production, at lower initial CH_4 levels for higher K_{zz}.

The exact K_{zz} profile of the Archean Earth is unclear; however, there was likely > 5,000 ppm of CH_4 in the atmosphere at 3.5 Ga (Catling & Zahnle 2020). For each of our simulations with an initial CH_4 abundance ≥ 5,000 ppm, regardless of the vertical mixing profile, we see HCN abundances > 1 ppm, and > 20 ppm for all but the CH_4 = 5,000 ppm, K_{zz} = 0.01x PAL case. These results hence suggest there would have been significant HCN production in

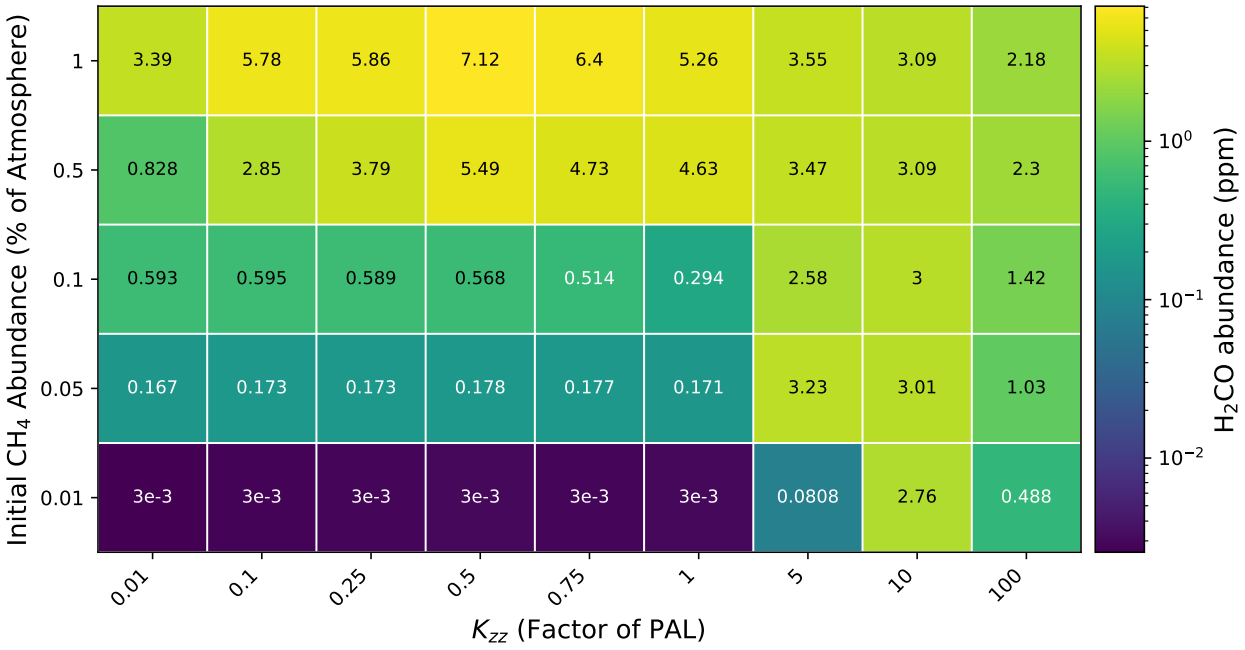

Figure 6. Vertically averaged H_2CO abundance for the full grid of Archean Earth simulations. Each square on the grid represents a simulation with a specific K_{zz} and initial CH_4 abundance value. The heat-map represents H_2CO abundance, with the values for each simulation shown in the squares in ppm.

a N_2-dominated Archean atmosphere with ~10% CO_2, subject to a plausible solar flux.

4.2.2 *H_2CO production*

We also plot the vertically averaged H_2CO abundances as a function of K_{zz} and the initial CH_4 abundance in Fig. 6. Many of the simulations produce H_2CO abundances > 3 ppm, and could hence lead to aqueous H_2CO concentrations of a few mM.

We see similar trends in H_2CO production as HCN production. When the K_{zz} profile is too low (typically ≤ 1.0x PAL), there is little production of H_2CO, < 1 ppm, for low initial CH_4 abundances. As K_{zz} increases, we generally see smaller jumps in H_2CO production between the 0.5% and 1.0% CH_4 simulations, up to the 100x PAL K_{zz} case, in which increasing the initial CH_4 abundance has a negative effect on H_2CO production. The reasoning behind this is not entirely clear, however, it is likely related to the Da number, and the competition between mixing and reaction timescales.

As with HCN, increasing K_{zz} loosens the CH_4 dependence of H_2CO production. Similarly, there is again a peak K_{zz} profile above which H_2CO production is decreased. We again use the CH_4 = 0.01% case for analysis. Firstly, comparing the K_{zz} = 1.0x and 10.0x PAL cases: the high K_{zz} case exhibits significantly higher H_2CO abundance, with a vertical average of 2.76 ppm, compared to 0.0808 ppm for the low K_{zz} case. The reaction rate plots for these simulations (Fig. A2(c - d)) show that only two out of the six most important reactions in the low K_{zz} case remain important for the high K_{zz} case, with the rates for both increasing substantially, particularly in the upper atmosphere. We also see significantly increased rates for reactions involving CH_x species, in particular $O + CH_3 \longrightarrow H_2CO + H$ and $H_2O + CH \longrightarrow H_2CO + H$. This is due to the increased availability of CH_x species in the upper atmosphere as a result of faster CH_4 replenishment, and more effective photochemical shielding from species such as C_2H_6.

The high K_{zz} case also shows an increase in reaction rates of several destruction pathways of H_2CO. The increased vertical mixing means that more H_2CO is in the photochemical region of the atmosphere and hence the rate of photolysis of H_2CO into $H_2 + CO$, and $H + HCO$ increases. The H_2CO also becomes more likely to react with CN, which forms HCN. However, there is a decrease in H_2CO destruction via atomic oxygen. As explained above, this is likely due to C_2H_6/CH_x species limiting the availability of O/O_2 in the atmosphere through their own reactions with atomic oxygen, and photochemical shielding.

Increasing K_{zz} from 10.0x to 100.0x PAL, we then see a decrease in H_2CO production, down to 0.488 ppm. This seems to be a result of two key reactions: there is a significant decrease in the rate of $HCO + HCO \longrightarrow H_2CO + CO$ in the lower atmosphere, as well as an increase in the rate of $H_2CO + CN \longrightarrow HCN + HCO$, particularly in the upper atmosphere. This is potentially caused again by changes to Da for each reaction. The production timescale of H_2CO is smaller than the destruction timescale. As a result, when K_{zz} is increased, the rate of production decreases relative to the rate of destruction.

4.2.3 *High-O_2 atmospheres*

Finally, we simulate an atmosphere composed of 65% CO_2, 34.99% N_2, and 0.01% CH_4, subject to the solar flux of the Archean Sun, and with an Archean Earth-like temperature-pressure profile and 10.0x the present-day Earth K_{zz} profile. Through the mechanisms outlined in §4.2.1 and 4.2.2, the high vertical mixing drives the production of 227.3 ppm HCN and 2.89 ppm H_2CO. These are in line with the aqueous concentrations of HCN and H_2CO shown to synthesise important biomolecules (§1.1). This is a significant result as it further demonstrates that high K_{zz} profiles can drive

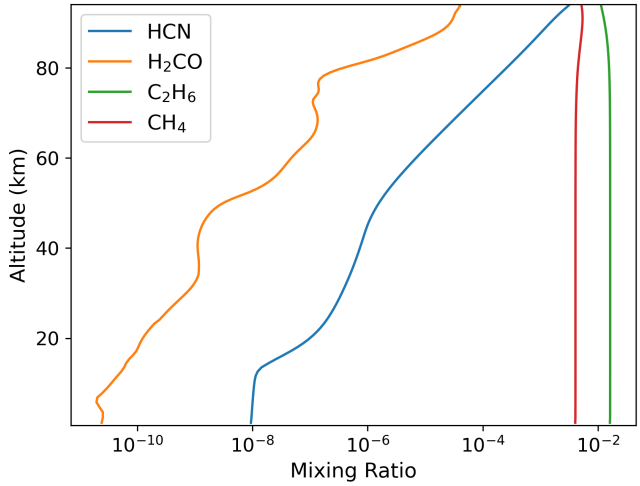

Figure 7. Abundance profiles for prebiotically significant compounds: HCN, H_2CO, C_2H_6, and CH_4, for a simulated Archean Earth atmosphere of 65% CO_2, 34.99% N_2, and 0.01% CH_4. Here, K_{zz} = 10.0x PAL.

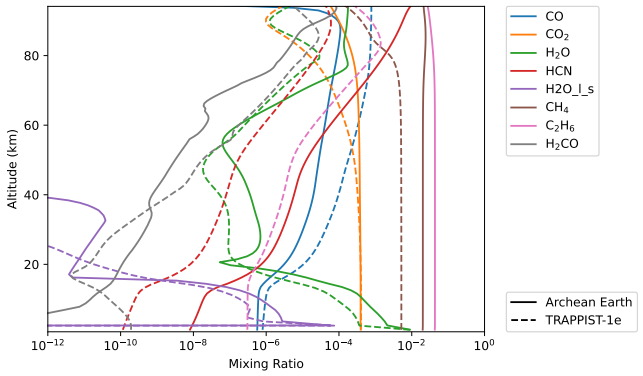

Figure 8. Abundance profiles of the Archean Earth (solid line) and TRAPPIST-1e (dashed line) atmospheres. Both simulations are initiated with 0.5% CH_4 and use K_{zz} = 1.0x PAL.

efficient production of HCN and H_2CO, and potentially important biomolecules, in atmospheres with C/O~0.5, and very low initial CH_4 abundances. Future work should aim to further test the attainable yields of HCN and H_2CO in oxidising atmospheres.

The findings in this subsection (§4.2) are consistent with Pearce et al. (2022), who also applied CRAHCN-O to the early Earth. They demonstrated that important biomolecule precursors, including HCN and H_2CO, can be produced photochemically in both reducing and oxidising early Earth atmospheres. Their results also find that the abundances of CH_4 and HCN are not necessarily dependent on the C/O ratio, given adequate CH_4 abundances. Our work extends this by demonstrating that even in CH_4-poor atmospheres, with C/O ratios close to 0.5, prebiotically significant amounts of HCN and H_2CO can accumulate if the K_{zz} profile is high.

4.3 TRAPPIST-1e

In this section, we first compare an initial TRAPPIST-1e simulation with the Archean Earth, for the same K_{zz} and initial CH_4 abundance. We then consider a reduced grid of experiments varying K_{zz} and initial CH_4 to examine whether the trends we see for the Archean in §4.2 are observed for TRAPPIST-1e.

4.3.1 Comparison with the Archean Earth

We compare the abundance profiles of the Archean and TRAPPIST-1e atmospheres in Fig. 8, for K_{zz} = 1.0x PAL and an initial CH_4 abundance of 0.5%. This shows the impact of changing the incident stellar flux, P-T profile, and atmospheric composition, as well as planetary parameters such as surface gravity.

There is less production of important prebiotic compounds, in particular C_2H_6, CH_4, and HCN, on TRAPPIST-1e. It is unclear from the abundance profile which simulation exhibits more efficient H_2CO synthesis; however, taking vertical averages of the mixing ratios, we find that there is 4.64 ppm of H_2CO in the Archean Earth atmosphere, compared to only 3.21 ppm for TRAPPIST-1e.

There is a higher intensity of Lyman-α incident on the TRAPPIST-1e atmosphere. As a result, we see significantly higher rates of C_2H_6 destruction via photolysis. Additionally, there is increased production of CH via photolysis, which in turn reacts with C_2H_6 to produce $C_2H_4 + CH_3$, and so further decreases C_2H_6 abundances. The rates of C_2H_6 production pathways are also reduced in the TRAPPIST-1e case, particularly at the top and bottom of the atmosphere. This is also explained by the higher Ly-α intensity. Although the increased destruction of C_2H_6 leads to increased production of its precursors, CH_x species, C_2H_4 etc., they are also being photolysed faster than they are being replenished. As in the high K_{zz} Archean Earth case, the mean altitude of C_2H_6 is considerably higher in the TRAPPIST-1e atmosphere. This negatively impacts the photochemical shielding effect of C_2H_6, further increasing the photolysis of its precursors. It also means that the majority of C_2H_6 precursors produced by its destruction form in the upper atmosphere, where the UV flux is higher.

HCN synthesis is significantly reduced in the lower TRAPPIST-1e atmosphere, and is almost zero near the surface. This is expected as key HCN precursors are photolysed in the upper atmosphere before vertical mixing can bring them closer to the surface. There is also a greater availability of CN in the TRAPPIST-1e atmosphere, formed through reactions between atomic nitrogen and CH_x species. CN reacts with (excited) atomic oxygen to form $N(^2D)$, excited atomic nitrogen. This leads to a significant increase in HCN destruction through $HCN + N(^2D) \longrightarrow N_2 + CH$.

H_2CO synthesis is impacted less by the harsher Ly-α. As for HCN, there is a decrease in production rates in the lower atmosphere due to the high photolysis rates of CH_x species higher in the atmosphere. We also see an increase in the destruction rates of H_2CO in the upper atmosphere through reactions with methane radicals.

4.3.2 K_{zz} and CH_4 dependence

The TRAPPIST-1e abundance grids (Fig. 9) show HCN abundances >1 ppm, but significantly below the 100 ppm (1 mM) threshold. However, these abundances could still be significant given the right concentration mechanisms, e.g. evaporation, and are still often above the significance threshold outlined in Rimmer & Rugheimer (2019). H_2CO production does exceed the 3 ppm threshold for significant aqueous concentrations via rain-out.

We also see similar trends to those observed for the Archean Earth atmosphere. The relationship between initial CH_4 abundance and HCN/H_2CO production is as in Fig. 5 and 6; increasing CH_4 generally increases the vertically averaged abundances of both compounds, except for HCN in the K_{zz} = 100.0x PAL case. At very high K_{zz},

HCN production does not scale as much as destruction. This is because increased CH_4 photolysis produces more CH_x radicals and CN, which are two key HCN sinks. We do not see this behaviour at lower K_{zz} as smaller amounts of CH_4 are brought up to the top of the atmosphere where the UV intensity is higher. Interestingly, for K_{zz} = 1.0x PAL, we see higher production of both HCN and H_2CO for initial CH_4 = 0.05% than for CH_4 = 0.10%. In the lower CH_4 case, C_2H_6 forms at a slightly higher altitude and is more effective at shielding the HCN and CH_x species from photolysis. For the 0.10% CH_4 case, C_2H_6 accumulates lower in the atmosphere, and the increased availability of initial CH_4 increases the amount of CH_x radicals in the photochemical region of the atmosphere, which are destroyed via photolysis.

The relationship between HCN/H_2CO production and K_{zz} also agrees with our Archean Earth results. As K_{zz} increases, so do HCN/H_2CO abundances, up to some value of K_{zz}, after which the increasing K_{zz} harms HCN/H_2CO production. This behaviour is driven by two key mechanisms on TRAPPIST-1e. Firstly, as K_{zz} becomes very high, the mixing timescale decreases more than the reaction timescale of HCN/H_2CO production. The second mechanism, which is more apparent for TRAPPIST-1e than the Archean Earth, is that the increased mixing brings more important HCN/H_2CO precursors to the top of the atmosphere, where the Ly-α intensity is very high. As discussed previously, this leads to the photodissociation of important species before they are able to form HCN or H_2CO.

Whilst the overall trends in Fig. 9 are the same as the Archean Earth results, there are some key differences. Firstly, we see peak HCN and H_2CO production at K_{zz} =10.0x PAL, compared to 1.0x and 0.50x PAL, respectively, for the Archean Earth. This is likely due to the higher intensity of Ly-α and less effective photochemical shielding on TRAPPIST-1e; more replenishment of HCN/H_2CO precursors is required to reach peak production.

The use of a finer grid of K_{zz} and initial CH_4 abundances in future work would allow for a more complete picture of the non-monotonic relationship between HCN/H_2CO production and K_{zz}/CH_4. However, the agreement between our results for the Archean Earth and TRAPPIST-1e, even for a reduced set of experiments, implies that we may see these behaviours in other planetary atmospheres.

4.4 Limitations

There are several limitations to this study, a number of which we discuss here. As previously stated, there is uncertainty around the atmospheric composition of the Archean Earth and TRAPPIST-1e, and hence their respective P-T profiles. We used fixed P-T and K_{zz} profiles. In reality, the P-T/K_{zz} profile of the atmosphere will determine the chemistry, which will in turn change the P-T/K_{zz} profile. For a more complete model, the existing VULCAN CRAHCN-O implementation should be paired with a radiative transfer code to calculate the updated profiles as the chemistry evolves. Our model is also 1-d, and hence fails to take into account horizontal transport and day-night contrasts (particularly important for the tidally locked TRAPPIST-1e). The development of a 3-D model would allow for much more considerate treatment of atmospheric dynamics.

Our analysis also has limitations. We take vertical column averages for the mixing ratios of species. As a result the structure of the species abundance profiles is not necessarily clear and can lead to misinterpretation. Additionally, when considering the abundances required to produce meaningful aqueous concentrations of HCN and H_2CO, we use a simple form of Henry's law at a reference temperature of 298.15 K. In actuality, the solubility of a compound is dependent on its temperature, among other things, and for a more accurate picture of aqueous concentrations the temperature dependent version of Henry's law should be used. Finally, we use the Damköhler number as a qualitative tool when considering the competition between mixing and reaction timescales in the atmosphere. This would be improved by a more careful analysis, which computes Da for key reactions in each simulation.

5 CONCLUSIONS

This study applied the VULCAN photochemical kinetics code with the recently implemented CRAHCN-O chemical network to the Archean Earth and TRAPPIST-1e, to investigate the production of HCN and H_2CO, important precursors to biomolecules. The findings of this study show that a high vertical mixing profile is able to drive the production of HCN and H_2CO in prebiotically significant abundances. Archean Earth yields are often >1 ppm, and up to 900 ppm for HCN, and up to 7.12 ppm for H_2CO. We see reduced abundances in the TRAPPIST-1e simulations: up to 19 and 5 ppm of HCN and H_2CO, respectively. This is due to the increased Ly-α of TRAPPIST-1 compared to the 3.8 Ga Sun, which increases the photolysis rate of destruction of important HCN/H_2CO precursors. For both planets, however, these are prebiotically significant abundances, even for seemingly low initial CH_4 abundances and C/O ratios. This greatly loosens the CH_4 requirement for efficient HCN production on the Archean Earth. We find that HCN and H_2CO production is non-monotonic in K_{zz}, initially increasing with increasing K_{zz} due to heightened replenishment of CH_x radicals to the upper atmosphere, before decreasing as the mixing timescale becomes less than the chemical reaction timescales.

This study necessarily makes several assumptions about the atmospheric composition and climate of the early Earth. Where possible, we have adopted the most recent constraints to ensure our results are well-informed. Future work could extend this study in various directions. Further study of HCN and H_2CO synthesis in oxidising atmospheres is required to test whether vertical mixing can consistently drive production in such an atmosphere. The implementation of a finer grid of K_{zz} and initial CH_4 abundance would better characterise the relationship between vertical mixing, CH_4 availability, and HCN/H_2CO production. Combining our results with atmospheric forward models such as TauREx or the Planetary Spectrum Generator would enable the calculation of transmission spectra, aiding to inform predictions for current and future exoplanet observations. Finally, coupling our 1-D photochemical model to radiative transfer codes and 3-D GCMs would allow for more careful treatment of atmospheric mixing and photolysis, as well as more frequent updates to the P-T/K_{zz} profiles as atmospheric chemistry evolves.

CODE AVAILABILITY

VULCAN (Tsai et al. 2017, 2021) is available on GitHub: https://github.com/exoclime/VULCAN (last access: 18 August 2025). Atmodeller (Bower et al. 2025) is available on GitHub: https://github.com/ExPlanetology/atmodeller/tree/main (last access 18 August 2025).

DATA AVAILABILITY

The data produced in this work are available at https://universityofexeteruk-my.sharepoint.com/:f:/g/personal/kf386_exeter_ac_uk/

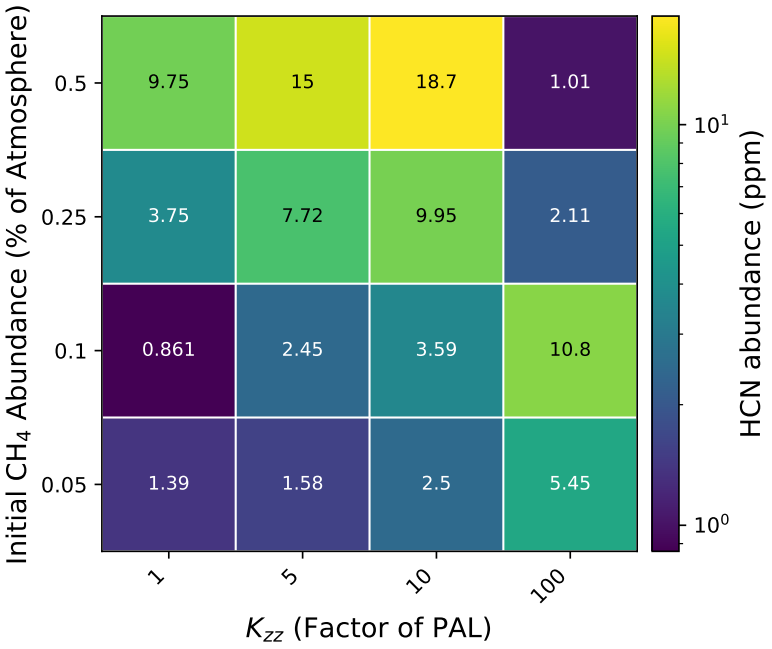

(a)

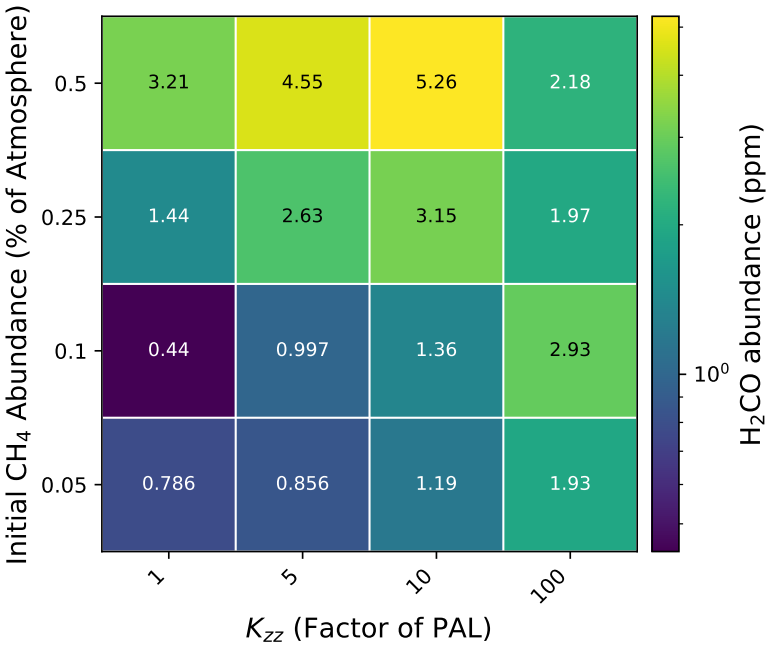

(b)

Figure 9. Vertically averaged a) HCN and b) H_2CO abundances for the full grid of TRAPPIST-1e simulations. Each square on the grid represents a simulation with a specific K_{zz} and initial CH_4 abundance value. The heat-map represents HCN/H_2CO abundance, with the values for each simulation shown in the squares in ppm.

ErkxiJv8SEtGkvUXU3thXu0B8hVFOIBhzvfibMdB7gTKow?e=2Blt8u. THAI data have been obtained from https://ckan.emac.gsfc.nasa.gov/organization/thai, a data repository of the Sellers Exoplanet Environments Collaboration (SEEC), which is funded in part by the NASA Planetary Science Divisions Internal Scientist Funding Model.

REFERENCES

Ardaseva A., Rimmer P. B., Waldmann I., Rocchetto M., Yurchenko S. N., Helling C., Tennyson J., 2017, Mon. Not. R. Astron. Soc., 470, 187

Atreya S. K., 1986, Vertical Mixing. Springer

Bennett J. A., Campbell Z. S., Abolhasani M., 2019, Current Opinion in Chemical Engineering, 26, 9

Bower D. J., Thompson M. A., Hakim K., Tian M., Sossi P. A., 2025,

Diversity of rocky planet atmospheres in the C-H-O-N-S-Cl system with interior dissolution, non-ideality, and condensation: Application to TRAPPIST-1e and sub-Neptunes (arXiv:2507.00499), https://arxiv.org/abs/2507.00499
Bradbury J., Frostig R., Hawkins P., 2018, JAX: composable transformations of Python+NumPy programs, 0.3.13., http://github.com/jax-ml/jax
Burkholder J. B., et al., 2015, Technical Report JPL Publication 15-10, Chemical Kinetics and Photochemical Data for Use in Atmospheric Studies, Evaluation No. 18, https://jpldataeval.jpl.nasa.gov. Jet Propulsion Laboratory, Pasadena, https://jpldataeval.jpl.nasa.gov
Burkholder J. B., et al., 2019, Technical Report JPL Publication 19-5, Chemical Kinetics and Photochemical Data for Use in Atmospheric Studies, Evaluation No. 19, https://jpldataeval.jpl.nasa.gov. Jet Propulsion Laboratory, Pasadena, https://jpldataeval.jpl.nasa.gov
Catling D. C., Zahnle K. J., 2020, Sci. Adv., 6, eaax1420
Claire M. W., Sheets J., Cohen M., Ribas I., Meadows V. S., Catling D. C., 2012, Astrophys. J., 757, 95
Cleaves II H. J., 2012, Evolution (N. Y.), 5, 342
Coulombe L.-P., et al., 2023, Nature, 620, 292
Eager-Nash J. K., et al., 2024, Mon. Not. R. Astron. Soc., 531, 468
Fauchez T. J., et al., 2020a, Geosci. Model Dev., 13, 707
Fauchez T. J., et al., 2020b, Geosci. Model Dev., 13, 707
Fauchez T. J., et al., 2022, Planet. Sci. J., 3, 213
Ferris J. P., Hill Jr A. R., Liu R., Orgel L. E., 1996, Nature, 381, 59
Feulner G., 2012, Reviews of Geophysics, 50
France K., Froning C., Behr P., Duvvuri G., Loyd P., Wilson D., Youngblood A., 2016, Measurements of the Ultraviolet Spectral Characteristics of Low-mass Exoplanetary Systems ("MUSCLES"), doi:10.17909/T9DG6F
Gillon M., et al., 2017, Nature, 542, 456
Gough D. O., 1981, Sol. Phys., 74, 21
Greene T. P., Line M. R., Montero C., Fortney J. J., Lustig-Yaeger J., Luther K., 2016, Astrophys. J., 817, 17
Grimm S. L., et al., 2018, Astron. Astrophys., 613, A68
Heays A. N., Bosman A. D., van Dishoeck E. F., 2017, Astron. Astrophys., 602, A105
Henry W., 1803, Philos. Trans. R. Soc. Lond., 93, 29
Johnson J. E., Gerpheide A., Lamb M. P., Fischer W. W., 2014, Geol. Soc. Am. Bull., 126, 813
Kadoya S., Catling D. C., 2019, Geochimica et Cosmochimica Acta, 262, 207
Krilanovic M., 2025, From Surface to Spectra: Characterizing TRAPPIST-1e's Atmosphere and Climate, doi:https://doi.org/10.5194/egusphere-egu25-19977
Lepot K., 2020, Earth-Science Reviews, 209, 103296
Martini J., 1994, Precambrian Research, 67, 159
Massie S. T., Hunten D. M., 1981, J. Geophys. Res., 86, 9859
Pearce B. K. D., Ayers P. W., Pudritz R. E., 2020a, J. Phys. Chem. A, 124, 8594
Pearce B. K. D., Molaverdikhani K., Pudritz R. E., Henning T., Hébrard E., 2020b, Astrophys. J., 901, 110
Pearce B. K. D., Molaverdikhani K., Pudritz R. E., Henning T., Cerrillo K. E., 2022, Astrophys. J., 932, 9
Pinto J. P., Gladstone G. R., Yung Y. L., 1980, Science, 210, 183
Rimmer P. B., Rugheimer S., 2019, arXiv [astro-ph.EP]
Rimmer P. B., Shorttle O., 2019, Origin of life's building blocks in Carbon and Nitrogen rich surface hydrothermal vents (arXiv:1901.08542), https://arxiv.org/abs/1901.08542
Ruiz-Bermejo M., Zorzano M.-P., Osuna-Esteban S., 2013, Life (Basel), 3, 421
Saha S., Basak S., Safonova M., Bora K., Agrawal S., Sarkar P., Murthy J., 2018, Astronomy and Computing, 23, 141
Sanchez R. A., Ferbis J. P., Orgel L. E., 1967, Journal of Molecular Biology, 30, 223
Sanchez R. A., Ferris J. P., Orgel L. E., 1968, J. Mol. Biol., 38, 121
Sander R., 2023, Atmos. Chem. Phys., 23, 10901
Sergeev D. E., et al., 2022, Planet. Sci. J., 3, 212
Som S. M., Buick R., Hagadorn J. W., Blake T. S., Perreault J. M., Harnmeijer J. P., Catling D. C., 2016, Nat. Geosci., 9, 448
Tian F., Kasting J. F., Zahnle K., 2011, Earth Planet. Sci. Lett., 308, 417
Tsai S.-M., Lyons J. R., Grosheintz L., Rimmer P. B., Kitzmann D., Heng K., 2017, The Astrophysical Journal Supplement Series, 228, 20
Tsai S.-M., Malik M., Kitzmann D., Lyons J. R., Fateev A., Lee E., Heng K., 2021, The Astrophysical Journal, 923, 264
Tsai S.-M., et al., 2023, Nature, 617, 483
Veillet R., Venot O., Sirjean B., Bounaceur R., Glaude P.-A., Al-Refaie A., Hébrard E., 2023, arXiv [astro-ph.EP]
Weber A. L., 1998, Orig. Life Evol. Biosph., 28, 259
Ysebaert T., Koch K., Samson R., Denys S., 2021, Urban For. Urban Greening, 59, 127014
Zahnle K. J., 1986, Journal of Geophysical Research: Atmospheres, 91, 2819
de Wit M. J., Furnes H., 2016, Sci. Adv., 2, e1500368

APPENDIX A: ABUNDANCE AND REACTION RATES PLOTS

To visualise the vertically averaged mixing ratios of various chemical species, as well as their mean altitudes in the atmosphere, we produce plots such as those shown in Fig. A1. The addition of the mean altitudes aids interpretation of our results, as the abundances alone are not indicative of the structure species take within the atmosphere. The dominant production and destruction pathways for a species can be seen using plots such as those shown in Fig. A2. The python script used to produce these scripts is included in the Data Availability. Here, we include the abundance and reaction rate plots used to justify how increased K_{zz} is able to drive efficient HCN and H_2CO production in a 0.01% CH_4 atmosphere by increasing the availability of CH_x radicals and C_2H_6 in the upper atmosphere.

This paper has been typeset from a TEX/LATEX file prepared by the author.

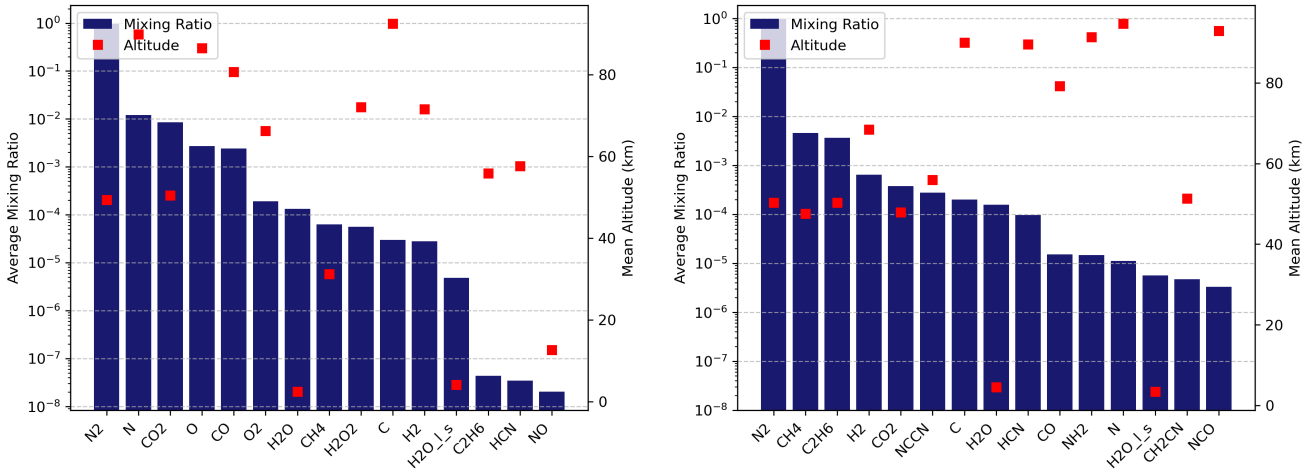

[H]

Figure A1. Bar charts showing the most abundant species in the Archean Earth atmosphere for simulations with an initial CH_4 abundance of 0.01% and K_{zz} = (a) 1.0x, and (b) 10.0x PAL.

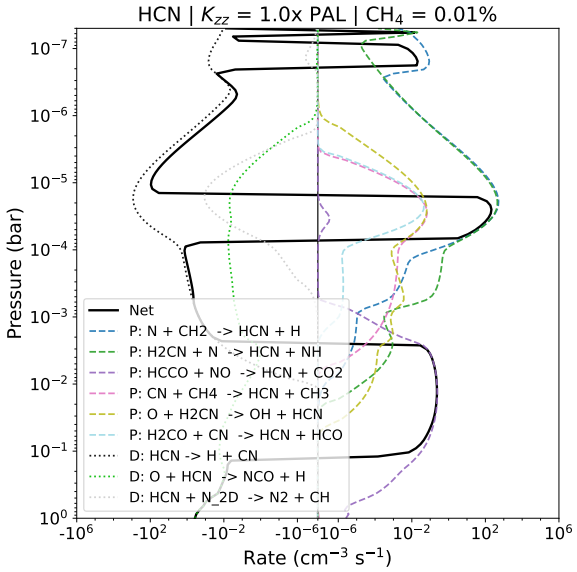
HCN | K_{zz} = 1.0x PAL | CH_4 = 0.01%
Pressure (bar)
Rate (cm^{-3} s^{-1})
Net
P: N + CH2 -> HCN + H
P: H2CN + N -> HCN + NH
P: HCCO + NO -> HCN + CO2
P: CN + CH4 -> HCN + CH3
P: O + H2CN -> OH + HCN
P: H2CO + CN -> HCN + HCO
D: HCN -> H + CN
D: O + HCN -> NCO + H
D: HCN + N_2D -> N2 + CH

(a)

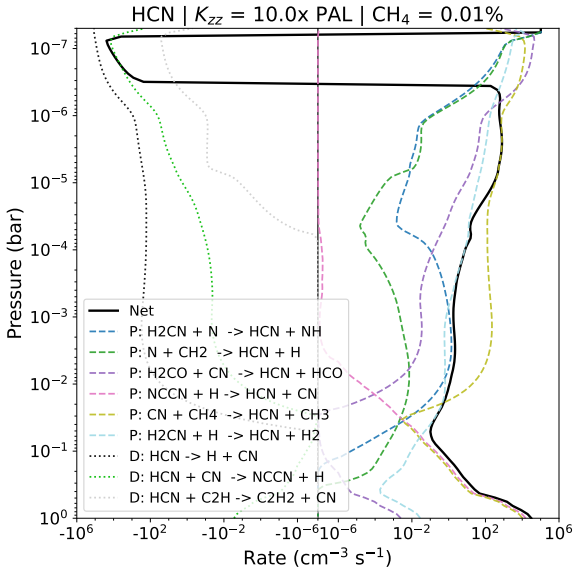
HCN | K_{zz} = 10.0x PAL | CH_4 = 0.01%
Pressure (bar)
Rate (cm^{-3} s^{-1})
Net
P: H2CN + N -> HCN + NH
P: N + CH2 -> HCN + H
P: H2CO + CN -> HCN + HCO
P: NCCN + H -> HCN + CN
P: CN + CH4 -> HCN + CH3
P: H2CN + H -> HCN + H2
D: HCN -> H + CN
D: HCN + CN -> NCCN + H
D: HCN + C2H -> C2H2 + CN

(b)

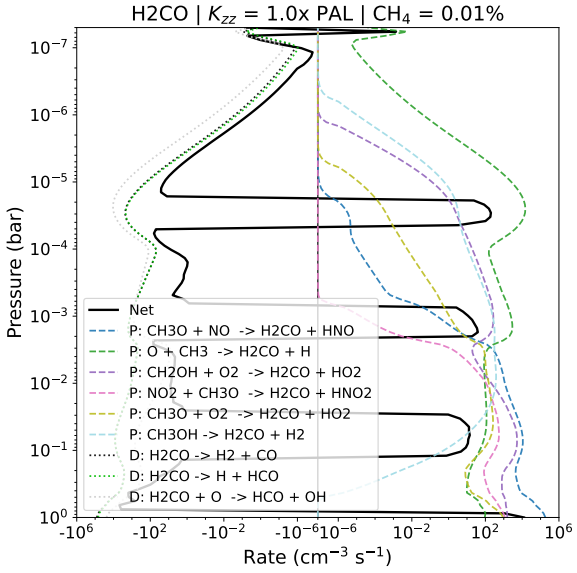
H2CO | K_{zz} = 1.0x PAL | CH_4 = 0.01%
Pressure (bar)
Rate (cm^{-3} s^{-1})
Net
P: CH3O + NO -> H2CO + HNO
P: O + CH3 -> H2CO + H
P: CH2OH + O2 -> H2CO + HO2
P: NO2 + CH3O -> H2CO + HNO2
P: CH3O + O2 -> H2CO + HO2
P: CH3OH -> H2CO + H2
D: H2CO -> H2 + CO
D: H2CO -> H + HCO
D: H2CO + O -> HCO + OH

(c)

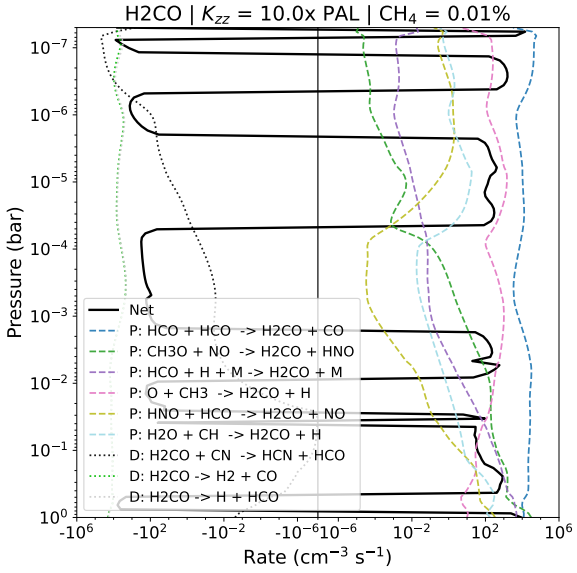
H2CO | K_{zz} = 10.0x PAL | CH_4 = 0.01%
Pressure (bar)
Rate (cm^{-3} s^{-1})
Net
P: HCO + HCO -> H2CO + CO
P: CH3O + NO -> H2CO + HNO
P: HCO + H + M -> H2CO + M
P: O + CH3 -> H2CO + H
P: HNO + HCO -> H2CO + NO
P: H2O + CH -> H2CO + H
D: H2CO + CN -> HCN + HCO
D: H2CO -> H2 + CO
D: H2CO -> H + HCO

(d)

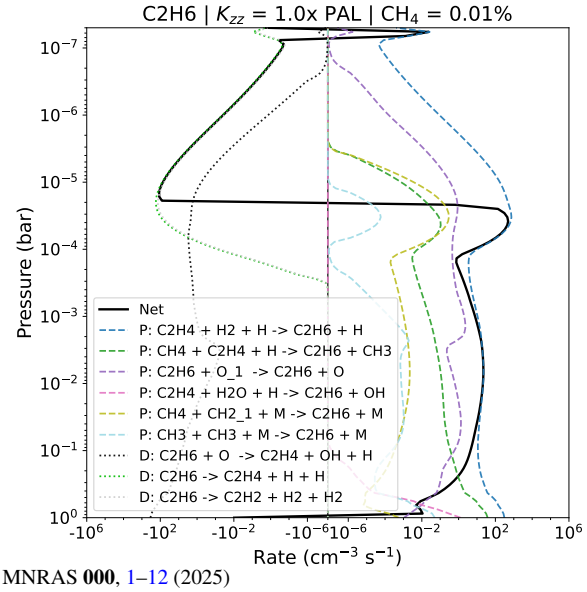
C2H6 | K_{zz} = 1.0x PAL | CH_4 = 0.01%
Pressure (bar)
Rate (cm^{-3} s^{-1})
Net
P: C2H4 + H2 + H -> C2H6 + H
P: CH4 + C2H4 + H -> C2H6 + CH3
P: C2H6 + O_1 -> C2H6 + O
P: C2H4 + H2O + H -> C2H6 + OH
P: CH4 + CH2_1 + M -> C2H6 + M
P: CH3 + CH3 + M -> C2H6 + M
D: C2H6 + O -> C2H4 + OH + H
D: C2H6 -> C2H4 + H + H
D: C2H6 -> C2H2 + H2 + H2

(e)

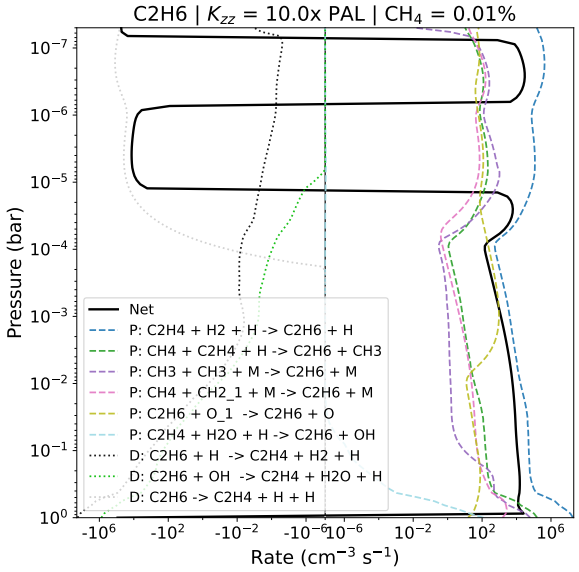
C2H6 | K_{zz} = 10.0x PAL | CH_4 = 0.01%
Pressure (bar)
Rate (cm^{-3} s^{-1})
Net
P: C2H4 + H2 + H -> C2H6 + H
P: CH4 + C2H4 + H -> C2H6 + CH3
P: CH3 + CH3 + M -> C2H6 + M
P: CH4 + CH2_1 + M -> C2H6 + M
P: C2H6 + O_1 -> C2H6 + O
P: C2H4 + H2O + H -> C2H6 + OH
D: C2H6 + H -> C2H4 + H2 + H
D: C2H6 + OH -> C2H4 + H2O + H
D: C2H6 -> C2H4 + H + H

(f)